Biomedicine & Pharmacotherapy 200 (2026) 119636

Contents lists available at ScienceDirect

Biomedicine & Pharmacotherapy

journal homepage: www.elsevier.com/locate/biopha

Purine derivatives as potential agents against Chagas disease: *Ex vivo*, *in vitro*, *in silico* evaluation, and identification of targets in *Trypanosoma cruzi*

Thalía Delgado [a,b], Alonzo González-González [c], Mercedes Didier Garnham [d,e], Emir Salas-Sarduy [d,e], Gildardo Rivera [c,*], Victoria Alonso [f,g], Esteban Serra [f,g], Rogelio Gómez-Escobedo [h], Jean-Luc Bertrand [a], Benjamín Nogueda-Torres [h], Cristian O. Salas [a,b,*]

[a] *Departamento de Química Orgánica, Facultad de Química y de Farmacia, Pontificia Universidad Católica de Chile, Santiago 702843, Chile*
[b] *Medicinal Chemistry Lab, Facultad de Química y de Farmacia, Pontificia Universidad Católica de Chile, Santiago 702843, Chile*
[c] *Laboratorio de Biotecnología Farmacéutica, Centro de Biotecnología Genómica, Instituto Politécnico Nacional, Reynosa 88710, Mexico*
[d] *Instituto de Investigaciones Biotecnológicas Dr. Rodolfo Ugalde (IIBIO), CONICET, San Martín, Buenos Aires 1650, Argentina*
[e] *Escuela de Bio y Nanotecnología (EByN), Universidad Nacional de San Martín (UNSAM), San Martín, Buenos Aires 1650, Argentina*
[f] *Facultad de Ciencias Bioquímicas y Farmacéuticas, Universidad Nacional de Rosario, Rosario, Santa Fe 2000, Argentina*
[g] *Instituto de Biología Molecular y Celular Rosario (IBR), Consejo Nacional de Investigaciones Científicas y Técnicas (CONICET)-UNR, Ocampo y Esmeralda, Rosario, Santa Fe CP 2000, Argentina*
[h] *Departamento de Parasitología, Escuela Nacional de Ciencias Biológicas Instituto Politécnico Nacional, Ciudad de México 07738, Mexico*

ARTICLE INFO

Keywords:
Trypanosoma cruzi
Purine derivatives
Cruzipain inhibitors
Bromodomain factor 2 inhibitors
In silico studies

ABSTRACT

Chagas disease, caused by *Trypanosoma cruzi*, affects millions of people worldwide and remains inadequately treated because the currently available drugs, benznidazole (Bzn) and nifurtimox (Nfx), show variable efficacy and significant toxicity across different disease stages. Given that purine nucleoside analogues have demonstrated antitrypanosomal activity and may target essential parasite proteins such as cruzipain (*Tc*CZP) and bromodomain factor 2 (*Tc*BDF2), this study aimed to determine whether a set of 20 purine derivatives possessed antiparasitic properties in relation to these targets using *ex vivo*, *in vitro* and *in silico* approaches. The results indicated that, in a screening assay against circulating trypomastigotes from two Mexican strains of *T. cruzi* (NINOA and INC-5), most of these purines outperformed the reference drugs Nfx and Bzn, according to the half-maximal lethal concentration (LC_{50}) values (which ranged from 6.28 to 144 μM for the NINOA strain and from 18.42 to 166.87 μM for the INC-5 strain), with the most active purines being the most active purines **9e**, **9i**, **9j**, **9m**, **9n**, and **9t**. Structure-activity relationship (SAR) analyses explained the influence of some fragments in the purine scaffold related to the trypanocidal effect. Subsequently, selected purines were tested against intracellular Tulahuen-2 amastigotes, where four demonstrated activities at sub-10 μM concentrations, and **9m** achieved approximately 1.5-fold greater potency than Bzn. Due to the low inhibitory activity of the purines tested against *Tc*CZP (the best compound, **9j**, had an IC_{50} of 87.1 μM), this target was ruled out as the source of the trypanocidal activity. However, when the compounds were evaluated on *Tc*BDF2, the results showed that **9i** and **9t** were the two best compounds with binding capacities to *Tc*BDF2 (K_d = 13.5 and 19.6 μM, respectively), which was more closely aligned with trypanocidal activity. In addition, **9i** and **9t** did not bind to *Tc*BDF3, indicating selectivity among these targets. Molecular docking and 200 ns molecular dynamics simulations supported the stable binding of purine **9i** to the *Tc*BDF2 bromodomain pocket. In addition, purines **9i**, **9j**, **9m**, and **9t** were predicted to have good pharmacokinetic profiles for oral administration of the drug. Overall, trisubstituted purines emerged as promising antichagasic leads, with *Tc*BDF2 engagement appearing more consistent with the observed trypanocidal activity, thereby guiding future optimisation towards a balance of potency, selectivity, and cytotoxicity.

* Corresponding author at: Departamento de Química Orgánica, Facultad de Química y de Farmacia, Pontificia Universidad Católica de Chile, Santiago 702843, Chile.
E-mail address: cosalas@uc.cl (C.O. Salas).

https://doi.org/10.1016/j.biopha.2026.119636
Received 20 April 2026; Received in revised form 26 May 2026; Accepted 6 June 2026
Available online 9 June 2026

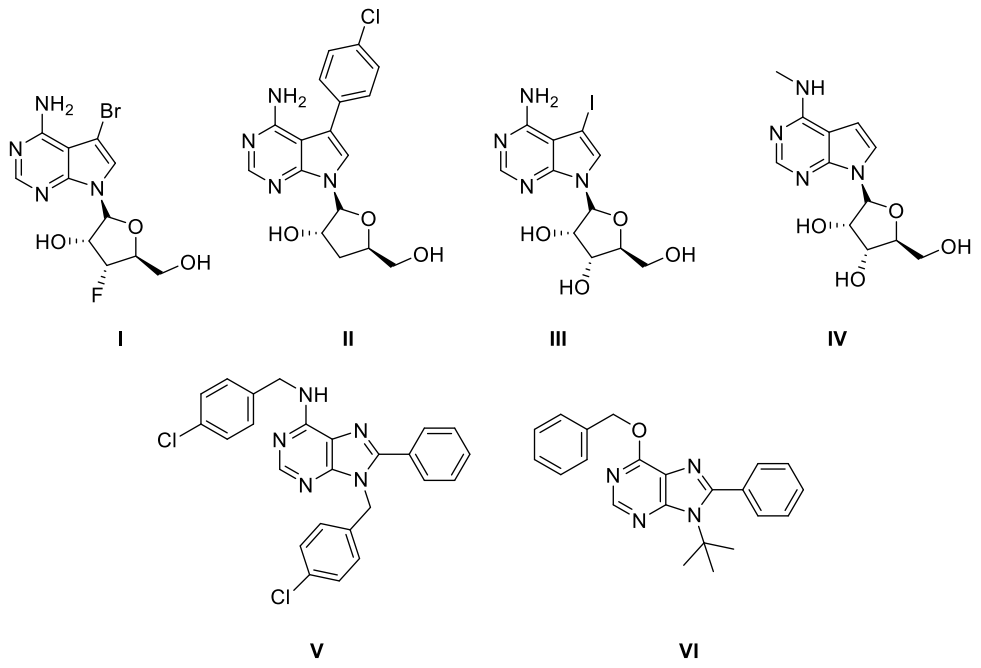

Fig. 1. Chemical structures of previously reported purines with trypanocidal activity.

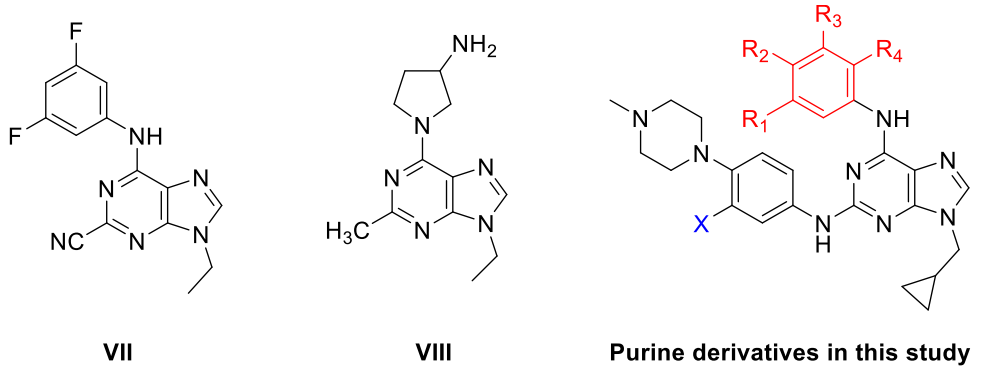

Fig. 2. Chemical structures of previously reported purine derivatives targeting *Tc*CZP (**VII**) and *Tc*BDF2 (**VIII**), together with the purine derivatives evaluated in this study.

1. Introduction

American trypanosomiasis or Chagas disease is a neglected tropical disease caused by the parasitic protozoan *Trypanosoma cruzi (T. cruzi)* [1]. Originally constrained within Latin American countries, recent emigration movements have spread the infection to other continents, affecting 6–7 million individuals worldwide. The two drugs currently available for treatment, benznidazole (Bzn) and nifurtimox (Nfx), show variable efficacy during the acute and chronic phases of infection and are frequently associated with adverse effects that may lead to treatment discontinuation [2,3]. Therefore, the development of safer and more effective therapeutic alternatives is necessary.

Purine nucleoside analogues exhibit a wide array of biological activities, including antiviral [4,5], antitumour [6,7], antibacterial [8,9], and antibacterial [8,9] activities, as well as antimycobacterial [10] activities. Some nucleoside derivatives, such as compounds **I–IV** (Fig. 1), have been reported to exhibit low micromolar and nanomolar activities against trypanosomatids, including African trypanosomes, *Leishmania spp.*, and *T. cruzi* [11–17]. To validate the importance of the purine scaffold in trypanocidal activity, several purine derivatives have been studied, including those synthesised and evaluated by Alonso-Padilla et al. [18,19]. Compounds **V** and **VI** (Fig. 1) showed activity against epimastigotes and amastigotes of *T. cruzi* at micromolar levels. **V** has an IC_{50} value of 5.16 μM on trypomastigotes and 187.50 μM on Vero cells, showing a high selective index (SI = 36), and an IC_{50} value of 4.20 μM on amastigotes [18]. In contrast, **VI** has an IC_{50} value of 5.56 μM for trypomastigotes and 3.78 μM for amastigotes [19].

In the search for targets for purine derivatives with anti-*T. cruzi* activities, cruzipain (CZP) protease has emerged as a potential therapeutic target. *Tc*CZP is an essential protease for parasite survival and functions in all its life stages, including host cell invasion, differentiation, and immune evasion [20,21]. Mott et al. [22] optimized the structural modification of heterocycles as small molecule nonpeptidic cruzipain inhibitors, resulting in purine **VII** (Fig. 2), with an IC_{50} value of 0.01 μM. **VII** was a competitive inhibitor, which was verified using the respective X-ray cruzipain-ligand complex. However, despite its potent *in vitro* activity, **VII** did not affect *T. cruzi* in cell cultures. Another promising target is bromodomain factor 2 (BDF2), an epigenetic reader involved in parasite proliferation and differentiation [23–25]. In their study, Tavernelli et al. screened a library of 28,251 compounds and selected seven as *Tc*BRD2 inhibitors. From this group, purine derivative **VIII** (Fig. 2) [23], which the *S*-stereoisomer showed a K_d of 1.33 μM, was the most promising. Nevertheless, despite its affinity for the bromodomain, this compound exhibited limited activity against *T. cruzi* epimastigotes (IC_{50}

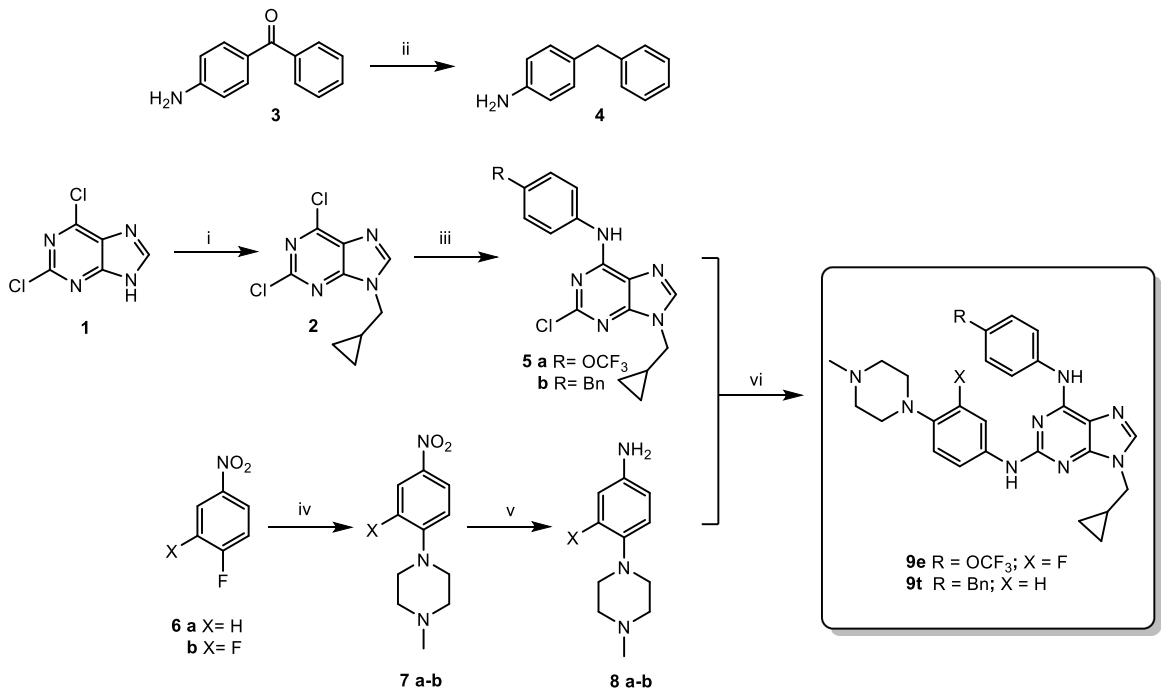

Scheme 1. Synthesis of purine derivatives **9e** and **9t**. *Reagents and conditions*: i) Methylcyclopropyl bromide, K_2CO_3, DMF, 12 h, rt, 60%. ii) Hydrazine, KOH, DEG, reflux, 8 h, 74%. iii) 4-(Trifluoromethoxy)-aniline or **4**, DIPEA, *n*-butanol, reflux, 12 h, 86–93%. iv) 1-Methyl-piperazine, K_2CO_3, DMF, rt, 98%. v) H_2, Pd-C, ethanol, rt, 4–6 h, quant. vi) K_2CO_3 2 M, $Pd(OAc)_2$, XantPhos, dioxane, MW (170 °C for 10 min), 67–74%.

> 10 μM).

Based on the trypanocidal effects of purine derivatives against the epimastigotes and trypomastigotes of *T. cruzi* and the possible involvement of potential targets, such as *Tc*CZP and *Tc*BDF2, in their mechanism of action, this study evaluated a series of purine derivatives as candidates for new drugs to treat Chagas disease. These purine derivatives were previously synthesised by our group and demonstrated interesting antiproliferative effects in haematological cancer cell lines [26,27], in line with the current trend toward reusing bioactive compounds, particularly in the case of trypanocidal and anticancer drugs [28]. These common mechanisms include the inhibition of cell proliferation, induction of lethal damage to rapidly dividing cells, oxidative stress induction, DNA damage through intercalation, topoisomerase inhibition, disruption of cell membranes, and activation of apoptosis [29–31]. This approach is fundamental in drug development programs that aim to identify new therapeutic applications for compounds previously investigated for other diseases [32]. Therefore, a set of 20 purine derivatives was evaluated for their biological effects against *T. cruzi* trypomastigotes of the INC-5 and NINOA strains. In addition, for the most promising compounds, the trypanocidal effect on amastigotes and viability effect on Vero cells were studied, and biochemical assays on proposed targets *Tc*CZP and *Tc*BDF2/*Tc*BDF3 were performed. *In silico* studies were also carried out to explain these biological results.

2. Methodology

2.1. Chemistry

Eighteen of the 20 purine derivatives assayed in this study were previously synthesised [26,27]. Two new purines (**9e** and **9t**) were synthesised according to the procedure shown in Scheme 1.

2.1.1. Synthesis of compounds 2

To a solution of 2,6-dichloro-9*H*-purine (**1**, 1.0 g, 5.29 mmol), methylcyclopropyl bromide (0.79 g, 5.82 mmol), and K_2CO_3 (2.19 g, 15.87 mmol) in DMF (10 mL), was added, and the mixture was stirred at room temperature for 12 h. The mixture was then filtered and evaporated. The residue was purified by silica gel chromatography using a polar mobile phase (EtOAc/hexane, 1:1) to obtain product **2**. White solid; yield 60%. The analytical data corresponded with those in the literature [27].

2.1.2. Synthesis of compound 4

To a solution containing **3** (500 mg, 2.53 mmol) in DEG (10 mL), hydrazine monohydrate (380 mg, 7.60 mmol) and KOH (427 mg, 7.60 mmol) were added, and the mixture was stirred under reflux overnight. Once the reaction was complete, 30 mL of water was added, and the mixture was extracted with chloroform (30 mL × 3), dried over anhydrous sodium sulphate, and concentrated to dryness on a rotary evaporator under reduced pressure to afford a black solid. The residue was purified by silica gel chromatography using a polar mobile phase (EtOAc/hexane, 1:1) to obtain product **4**. Orange solid, yield 74%, m.p. = 120–121 °C. ^{1}H NMR (200 MHz, Chloroform-*d*) δ 7.36–7.07 (m, 5H, 5 CH), 7.04–6.84 (m, 2H, 2 CH), 6.67–6.51 (m, 2H, 2 CH), 3.86 (s, 2H, CH_2), 3.50 (s, 2H, NH_2).

2.1.3. Synthesis of compounds 5a–b

To a solution of **2** (200 mg, 0.83 mmol), aniline (0.90 mmol), and DIPEA (0.3 mL, 1.65 mmol) in n-butanol (5 mL), the mixture was stirred at 150 °C for 12 h. To quench the reaction, ice water was added to the reaction mixture, extraction was carried out with EtOAc (3 × 15 mL), and the organic layer was dried using anhydrous Na_2SO_4 and concentrated. The residue was purified by silica gel chromatography using a polar mobile phase (AcOEt:hexane 60:40) to give products **5a–b**.

2-Chloro-9-(cyclopropylmethyl)-*N*-(4-(trifluoromethoxy)phenyl)-9*H*-purin-6-amine, (**5a**). White solid, yield 93%. The analytical data corresponded with those in the literature [26].

N-(4-benzylphenyl)-2-chloro-9-(cyclopropylmethyl)-9*H*-purin-6-amine (**5b**). Orange solid, yield 86%, m.p. = 146–147 °C. ^{1}H NMR (200 MHz, Chloroform-*d*) δ 7.90 (d, J = 4.3 Hz, 2H, 2 CH), 7.75–7.61 (m, 2H, 2 CH), 7.34–7.10 (m, 7H, 7 CH), 4.08–3.93 (m, 4 H, 2 CH_2), 1.32 (m, 1H, CH), 0.78–0.59 (m, 2 H, CH_2), 0.53–0.36 (m, 2 H, CH_2).

2.1.4. Synthesis of compounds 7a–b

To a solution of **6a-b** (1 g, 7.0 mmol), 1-methylpiperazine (7.1 mmol), and K_2CO_3 (2.9 g, 21.1 mmol) in DMF (10 mL), was added, and the mixture was stirred at room temperature for 12 h. The reaction mixture was then filtered and evaporated. The solid was then recrystallised from MeOH to give **7a–b.**

1-(2-Fluoro-4-nitrophenyl)-4-methylpiperazine, (**7a**). Yellow solid, 98%. The analytical data corresponded with the literature [27]. 1-Methyl-4-(4-nitrophenyl)piperazine (**7b**) Yellow solid, 98%. The analytical data corresponded with the literature [27].

2.1.5. Synthesis of compounds 8a–b

To a solution of **7a–b** (500 mg, 1.69 mmol), Pd-C (34 mg) in ethanol (10 mL) under a hydrogen atmosphere was added, and the mixture was stirred at room temperature for 12 h. After the completion of the reaction, the mixture was filtered through Celite and concentrated to afford **8a–b**. 3-Fluoro-4-(4-methylpiperazin-1-yl)aniline (**8a**). Purple solid, quant. The analytical data corresponded with the literature. 4-(4-Methylpiperazin-1-yl)aniline, (**8b**). Purple solid, quant. The analytical data corresponded with the literature [27].

2.1.6. Synthesis of final compounds 9e and 9t

To a solution of **5a–b** (200 mg, 0.49 mmol) and **8a–b** (132 mg, 0.59 mmol) in dioxane (5 mL), $Pd(OAc)_2$ (11 mg, 0.05 mmol, 0.1 eq), XantPhos (86 mg, 0.14 mmol, 0.3 eq), and 2 M K_2CO_3 (aq) (0.75 mL, 0.15 mmol, 3 eq) were added, and the mixture was stirred at 170 °C for 10 min in a microwave reactor (Anton Paar Monowave 200). After cooling to room temperature, the reaction mixture was filtered through celite, and the filtrate was diluted with dichloromethane and concentrated to dryness. The residue was purified by silica gel chromatography using a polar mobile phase (methanol/dichloromethane, 5:95 and 10:90) to obtain the final product. The Rf values of each compound were calculated using a 5:95 mobile phase ratio.

9-(Cyclopropylmethyl)-N^2-(3-fluoro-4-(4-methylpiperazin-1-yl) phenyl)-N^6-(4-(trifluoromethoxy)phenyl)-9*H*-purine-2,6-diamine (9e). Brown solid, yield 74%, m.p. = 172.0 – 172.6 °C. ^{1}H NMR (200 MHz, Chloroform-*d*) δ 8.08 (s, 1H, NH), 7.74 (d, J = 9.4 Hz, 3H, NH, 2 CH), 7.67 (d, J = 2.5 Hz, 1H, CH), 7.21–7.07 (m, 4H, 4 CH), 6.90 (t, J = 9.1 Hz, 1H, CH), 3.96 (d, J = 7.1 Hz, 2H, CH_2), 3.10 (t, J = 4.8 Hz, 4H, 2 CH_2), 2.64 (d, J = 4.7 Hz, 4H,2 CH_2), 2.37 (s, 3H, CH_3), 1.31 (m, J = 9.8, 8.0, 5.0 Hz, 1H, CH), 0.75–0.62 (m, 2H, CH_2), 0.52–0.38 (m, 2H, CH_2). ^{13}C NMR (50 MHz, Chloroform-*d*) δ 175.96, 156.05, 151.93, 151.19, 138.22 (d, $^1J_{C\text{-}F}$ = 243.5 Hz), 137.61, 135.55(d, $^2J_{C\text{-}F}$ = 20.9 Hz), 134.43 66 (d, $^3J_{C\text{-}F}$ = 9.4 Hz), 121.60 (2C), 121.35 (2C), 119.00, 115.39, 114.66, 108.30, 107.79, 55.22 (2C), 50.85, 48.24, 46.10, 11.01, 4.28 (2C). ESI/MS for ($C_{27}H_{28}F_4N_8O$ $[M+H]^+$): Calcd: 557.2322. Found: 557.2339.

N^6-(4-Benzylphenyl)-9-(cyclopropylmethyl)-N^2-(4-(4-methyl-piperazin-1-yl)phenyl)-9*H*-purine-,6-diamine (9t). Brown solid, yield 67%, m.p. = 260–262 °C. ^{1}H NMR (200 MHz, Chloroform-*d*) δ 7.85 (s, 1H, NH), 7.65 (d, J = 8.4 Hz, 2H, NH, CH), 7.58 – 7.49 (m, 2H, 2 CH), 7.30–7.11 (m, 8H, 8 CH), 6.90 (d, J = 9.3 Hz, 3H, 3 CH), 4.01–3.87 (m, 4H, 2 CH_2), 3.16 (dd, J = 6.2, 3.7 Hz, 4H, 2 CH_2), 2.61 (t, J = 4.9 Hz, 4H, 2 CH_2), 2.37 (s, 3H, CH_3), 1.26 (s, 1H, CH), 0.75–0.51 (m, 2H, CH_2), 0.43 (p, J = 5.7, 5.3 Hz, 2H, CH_2). ^{13}C NMR (50 MHz, Chloroform-*d*) δ 156.72, 152.12, 146.59, 141.33, 137.67, 137.09, 135.80, 133.32, 129.22, 128.88 (2C), 128.41 (2C), 125.99, 120.68, 120.53, 116.94 (2C), 115.08, 77.66, 77.02, 76.38, 55.17 (2C), 49.97 (2C), 48.10, 46.08, 41.34, 11.04, 4.26 (2C). ESI/MS for ($C_{33}H_{36}N_8$ $[M+H]^+$): Calcd: 545.3136. Found: 545.3144.

2.2. Trypanocidal activity against T. cruzi trypomastigotes

Female CD1 mice aged 6 – 8 weeks were infected with *T. cruzi* bloodstream trypomastigotes. The infection course was followed for 4 – 6 weeks. At the peak of parasitaemia (monitored every few days under a microscope), blood was drawn by cardiac puncture, and the sample was treated with sodium heparin as an anticoagulant to prevent blood clotting. The blood sample was adjusted to 1×10^6 bloodstream trypomastigotes/mL.

In a 96-well microplate, 195 μL of infected blood was added to each well along with 5 μL of a solution of purine derivatives and reference drugs at different concentrations to reach a final volume of 200 μL. Each concentration (3.25 – 50 μg/mL) was assayed in triplicate. Initially, all compounds were tested at a final concentration of 12.5 μg/mL (22.04–27.50 μM). Wells containing untreated trypomastigotes and 5% DMSO served as negative controls. Wells containing reference drugs were used as the positive controls. The microplates were then refrigerated at 4 °C for 24 h, and the bloodstream trypomastigotes were quantified using the Brenner–Pizzi method [33]. Five microlitres of the sample were placed on a microscope slide and covered with a 13 × 13 mm glass coverslip. The motile parasites were counted in 15 microscope fields at 40 × magnification using an optical microscope. The half-maximal lethal concentration (LC_{50}) was determined using the percentage of mortality calculated by comparing the untreated and treated wells. The half-maximal lethal concentration (LC_{50}) was determined using probit analyses.

2.3. Trypanocidal activity against T. cruzi Tul-2 amastigotes

To evaluate the trypanocidal activity of the investigational compounds, a colorimetric assay was performed using transgenic *T. cruzi* Tulahuen-2 parasites expressing *E. coli* β-galactosidase (LacZ) [34]. This strain was a generous gift from Dr. Frederick Buckner (University of Washington, USA). Vero cells were seeded at a density of 5×10^3 cells per well in 96-well plates using MEM medium supplemented with 10% foetal bovine serum (FBS). After 48 h, the cells were infected with 5×10^4 purified trypomastigotes per well (multiplicity of infection [MOI] =10) in MEM supplemented with 4% serum. Following a 24-h infection period, the cultures were washed twice with PBS to remove extracellular parasites and then incubated with RPMI medium without phenol red (Gibco #11835030), supplemented with 4% serum and drug dilutions (100–0.39 μM) of the tested compounds. Benznidazole (Bzn, 20–0.08 μM) was used as a positive control. A 0.5% DMSO vehicle control was also included in both infected/untreated and non-infected/untreated wells to establish the maximum and minimum expected β-galactosidase activity, respectively. The final DMSO concentration did not exceed 0.5% under any condition to avoid interference with the viability of the parasite or host cells. After 72 h of incubation with the compounds, 100 μL of a freshly prepared PBS solution containing 1% NP-40 and 100 μM CPRG (Roche #10884308001) was added to each well, resulting in final concentrations of 0.5% NP-40 and 50 μM CPRG, respectively. The plates were incubated for 4 h at 37 °C, protected from light. β-galactosidase activity was quantified by measuring the absorbance at 595 nm using a FilterMax F5 Multimode Microplate Reader.

2.4. Cytotoxicity determination against VERO cells

To evaluate the cytotoxicity of the compounds, a resazurin assay [35] was performed on non-infected Vero cell cultures using the same compound concentrations as in the trypanocidal assay described above. Vero cells were seeded at a density of 5×10^3 cells per well in 96-well plates and cultured in MEM medium supplemented with 10% foetal serum (FBS). After 48 h, the medium was replaced with MEM containing 4% serum to match the conditions used in the trypanocidal activity assay. Following an additional 24 h of incubation, the cells were washed twice with PBS and treated with fresh RPMI medium (4% serum) containing serial dilutions of each compound (100–0.39 μM). The cells were incubated under these conditions for 72 h. Bzn (range: 20–0.08 μM) was used as a viability control. A 0.5% DMSO vehicle control was included to establish the expected maximum resazurin reduction level. In all cases,

the final DMSO concentration was maintained at 0.5% to prevent any effect on cell viability. Subsequently, 10 μL of freshly prepared 10× (440 μM in PBS) resazurin solution was added to each well. After 7 h of incubation, the samples were transferred to a black 96-well plate, and fluorescence ($\lambda_{excitation/emission}$: 535 nm/595 nm) was measured using a FilterMax F5 Multimode Microplate Reader.

2.5. TcCZP inhibition assay

2.5.1. Cruzipain purification

Endogenous cruzipain, a complex mixture of glycosylated and closely related isoforms present in *T. cruzi* parasites, was purified from epimastigotes of the Tulahuen-2 strain, as described previously [36]. Purified enzyme was stored at −70 °C as individual aliquots for single use.

2.5.2. TcCZP assay

*Tc*CZP activity was assayed fluorometrically using the substrate Z-FR-AMC, as described previously [37]. In brief, Z-FR-AMC substrate (final concentration 1.63 μM) was added to a reaction mix containing *Tc*CZP (5.5 nM) in activity buffer (100 mM NaAc, 5 mM DTT, 2.5% DMSO, 0.01% Triton X-100 pH 5.5). The release of 7-amino-4-methylcoumarin was continuously monitored at 30 °C during 45–60 min in a FilterMax F5 Multimode Reader (Molecular Devices) using standard 340 nm excitation and 450 nm emission filter set. The slopes (dF/dt) of the progression curves were determined using linear regression analysis with GraphPad Prism software (version 5.03).

Compounds were tested in a dose-response manner (range: 500 μM - 0.49 μM) using the assay conditions described above. The irreversible inhibitor E-64 (*trans*-epoxysuccinyl-L-leucylamido-(4-guanidino) butane, range: 125–0.122 nM) was used as positive control. The compounds were initially pre-incubated at 30 °C with *Tc*CZP in the activity buffer for 20 min before adding the substrate. Data collection and processing were performed as described previously. The percentage of *Tc*CZP residual activity was calculated for each condition according to Eq. (1):

$$\%Res.\ Act. = 100 \cdot [(dF/dt - \mu C-)/(\mu C+ - \mu C-)] \quad (1)$$

where dF/dt represents the slope of each condition, and μC + and μC− are the averages of the *Tc*CZP (no-inhibition) and substrate (no-enzyme) controls, respectively. The half-maximal inhibitory concentration (IC_{50}) and Hill slope parameters for each compound were estimated by fitting the four-parameter Hill equation to the experimental data from the dose-response curves using GraphPad Prism software.

2.6. TcBDFs inhibition assay

2.6.1. Recombinant protein purification

The bromodomain from *Tc*BDF2 (*Tc*BD2) was purified under soluble conditions, as reported previously, from *E. coli* BL21 transformed with pDEST17-*Tc*BDF2. The recombinant protein was obtained by induction with 0.5 mM IPTG for 3 h at 37 °C [23]. The recombinant protein was purified using nickel-charged resin (Ni-NTA Agarose, Qiagen) according to the manufacturer's instructions. Correct folding was verified by Circular Dichroism spectroscopy using a spectropolarimeter (Jasco J-810; Easton, MD, USA). *Tc*BDF3 was purified under insoluble conditions and then refolded as previously described [38].

2.6.2. Thermal shift assay

*Tc*BDF2 (or *Tc*BDF3) was buffered in 10 mM HEPES (pH 7.5) and 500 mM NaCl and assayed in a 48-well plate at a final concentration of

Table 1
Trypanocidal activity of purine derivatives against *T. cruzi* trypomastigotes of the NINOA and INC-5 strains.

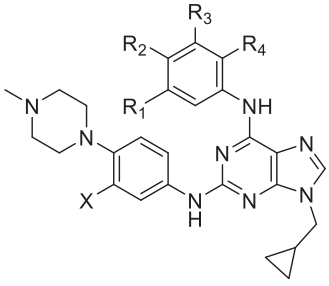

Compound	X	R_1	R_2	R_3	R_4	Trypanocidal activity LC_{50} (μM)	
						NINOA	INC-5
9a	F	H	F	H	H	76.15 ± 17.00	166.87 ± 25.13
9b	H	H	F	H	H	45.88 ± 6.35	58.58 ± 9.94
9c	H	H	H	H	H	49.77 ± 5.08	82.97 ± 11.46
9d	F	H	H	H	H	26.11 ± 3.30	94.78 ± 17.51
9e	F	H	OCF_3	H	H	16.40 ± 3.45	75.01 ± 7.78
9 f	F	H	OCH_3	H	H	45.60 ± 2.47	55.11 ± 3.90
9 g	H	H	Cl	OCH_3	H	78.94 ± 8.52	91.19 ± 12.45
9 h	F	H	Cl	OCH_3	H	50.68 ± 3.48	43.44 ± 3.71
9i	H	OCH_3	Cl	H	OCH_3	23.26 ± 1.56	24.08 ± 4.59
9j	F	OCH_3	Cl	H	OCH_3	50.10 ± 3.30	20.34 ± 3.78
9k	H	H	H	NO_2	H	49.57 ± 3.51	80.83 ± 14.99
9 l	H	H	H	CH_3	H	62.86 ± 7.84	59.38 ± 9.05
9 m	H	H	OCF_3	H	H	13.14 ± 2.31	19.46 ± 4.27
9 n	H	H	H	OCF_3	H	13.40 ± 2.24	26.97 ± 1.57
9o	H	H	F	Cl	H	34.77 ± 3.59	41.44 ± 3.34
9p	H	H	Cl	Cl	H	144.08 ± 11.36	64.95 ± 9.87
9q	H	H	H	Cl	H	57.89 ± 4.86	45.07 ± 4.85
9r	H	H	H	CF_3	H	58.89 ± 7.53	45.29 ± 6.37
9 s	H	H	Cl	F	H	21.62 ± 3.22	25.08 ± 5.19
9 t	H	H	$CH_2C_6H_5$	H	H	6.28 ± 1.00	18.42 ± 4.87
Bzn						131.55 ± 29.13	190.11 ± 19.24
Nfx						70.68 ± 11.61	139.08 ± 12.96

2 μM in a 20 μL volume. The compounds were first tested at a fixed concentration of 5 μM. K_d values were subsequently determined for compounds producing shifts greater than 0.5 °C. Compounds **9i** and **9t** were added at final concentrations between 1 and 200 μM to determine the dissociation constants. SYPRO Orange (Invitrogen) was added as a fluorescent probe at a dilution of 1:1000. The excitation and emission filters for the SYPRO Orange dye were set at 465 and 590 nm, respectively. The temperature was increased in steps of 2 °C per minute from 25 °C to 96 °C, and fluorescence readings were taken at each interval in a CFX Opus 96 Real-Time System (Bio-Rad) and analysed using Maestro Software (Bio-Rad). The melting curves and average melting temperatures for each condition were obtained and plotted in temperature vs. concentration graphs using GraphPad Prism (version 9.0). The plots were fitted using the DSF single-binding site equation to obtain the dissociation constants (K_d), as previously reported [24].

2.7. Molecular docking

Molecular docking analysis was conducted to assess the potential of purine derivatives on two proposed pharmacological targets, *Tc*CZP and *Tc*BDF2, *respectively*. The ligand structures were drawn using Marvin Sketch 21.13 to obtain the SMILE code for each molecule, and each SMILE code was then 3D energy-minimised using Open Babel 3.1.1 software and saved in sdf format for subsequent use in molecular docking [39]. The two proposed protein were retrieved from the Protein Data Bank (PDB) using access codes 4W5B *T. cruzi* cruzain (*Tc*CZ) and 6NIM (*Tc*BDF2). Water molecules, co-crystalized ligands, and ions were removed from the protein structure and prepared for molecular docking using UCSF Chimera 1.15 software [40]. Molecular docking was conducted using the gnina 1.0.3 software for all purine derivatives and known inhibitors co-crystallised with each protein for comparison [41]. The interaction profile for each ligand–protein complex was calculated using the protein-ligand interaction profiler (PLIP) [42]. The compounds were analysed based on two criteria: the binding free energy (BFE) predicted by the docking software gnina and the interaction profiles calculated by PLIP.

2.8. Molecular dynamics simulation for TcBDF2

Molecular dynamics analyses were performed for purines **9i** to analyse the putative binding mode of the *Tc*BDF2 ligand, starting from the most stable binding pose predicted by molecular docking analysis. Molecular dynamics analysis was performed using the free-access software GROMACS version 2018 [43]. Initially, the topologies of **9i** were generated using ACPYPE with the General Amber Force Field (GAFF). The system was solvated with water molecules in a dodecahedron with a minimum wall distance of 10 Å using the TIP3 water model. Sodium and chloride ions were added as required to achieve a neutral charge in the system. The system was energy-minimised using a steepest descent algorithm. Two equilibrium steps were performed in this study. First, the compound was simulated under NVT conditions (constant number of particles, volume, and temperature). In the second step, the compound was simulated under NPT conditions (constant number of particles, pressure, and temperature). Each stage lasted 100 ps. The simulation was performed at 300 K for a trajectory of 200 ns [44]. The stability of the complex was determined using built-in GROMACS tools. The RMSD values for the α-carbons and ligands were then obtained. The RMSD matrix was calculated for the entire trajectory of the simulation. The RMSF of the α-carbons was calculated to understand the effect of the compound on the secondary structure of protein. Finally, the radius of gyration of complex was obtained to determine the stability of the complex and three-dimensional compactness of *Tc*BDF2.

3. Results and discussion

3.1. Trypanocidal activity against T. cruzi trypomastigotes and structure-activity relationship

The *ex vivo* activities of the purine derivatives against the NINOA and INC-5 strains of *T. cruzi* are summarised in Table 1. These strains, NINOA and INC-5, are Mexican isolates frequently used in research to study the high genetic and biological diversity of the parasite, particularly within the *Tc*I genotype (according to Discrete Typing Units, DTUs). This is an important point because *Tc*I predominates in the overall sample (~60% of strains) and is the most common cause of acute Chagas disease. It is widely distributed, particularly in South and Central America and Mexico [45].

Table 1 shows that the LC_{50} values ranged from 6.28 to 144 μM for the NINOA strain and 18.42–166.87 μM for the INC-5 strain. Nfx and Bzn were used as the controls. In general, regarding trypanocidal effect, 19 of the 20 compounds were more potent than Bzn (LC_{50} = 131.55 μM) against the NINOA strain, and 17 were more potent than Nfx (IC_{50} = 70.68 μM). Additionally, all compounds tested were more potent than Bzn (LC_{50} = 190.11 μM) against the INC-5 strain, and 19 were more potent than Nfx (LC_{50} = 139.08 μM). Therefore, a set of purine derivatives with a high capacity to inhibit the growth of *T. cruzi*

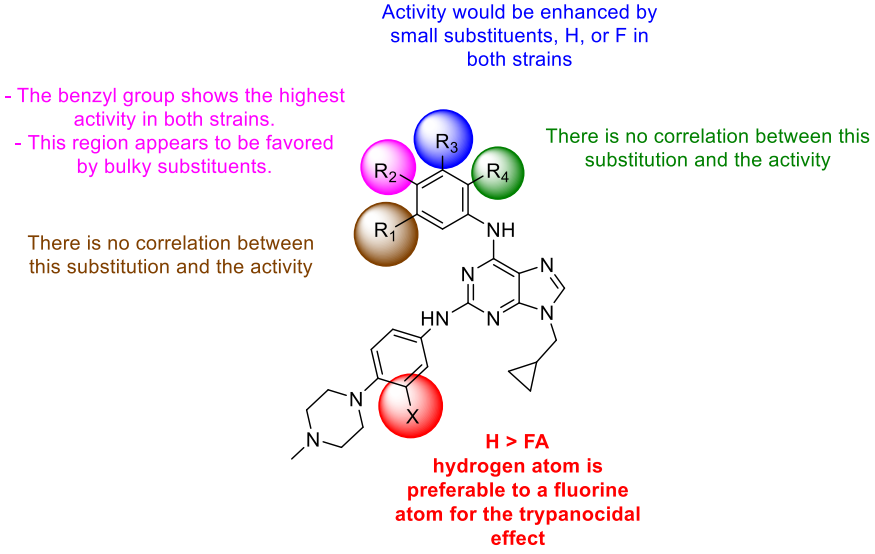

Fig. 3. Summary of the main SAR observed for trypanocidal effects on trypomastigotes of the NINOA and INC-5 strains for purine derivatives.

Table 2
Trypanocidal activity of the selected active purine derivatives against *T. cruzi* Tul-2 amastigotes and viability on Vero cells. Confidence intervals (95%) are presented in parentheses. The calculated selectivity index (SI) values were expressed.

Compound	CC_{50} Vero cells (μM)	IC_{50} Tul-2 amastigotes (μM)	SI[a]
9e	9.02 (6.67–12.18)	3.16 (2.79–3.57)	2.9
9i	11.40 (ND)	11.40 (7.62–17.07)	1.0
9j	11.00 (ND)	5.57 (5.01–6.17)	2.0
9m	12.20 (9.78–15.18)	1.89 (1.67–2.12)	6.5
9n	8.77 (6.93–11.09)	3.02 (2.57–3.53)	2.9
9t	13.12 (10.89–15.79)	3.56 (2.93–4.32)	3.7
Bzn	> 100 (ND)	2.92 (2.28–3.97)	> 34

ND: note determined.
[a] SI values were calculated as CC_{50}/IC_{50}.

trypomastigotes is shown here, in comparison with the reference drugs. It is crucial to recognize that trypomastigotes serve as a clinically significant model, as they represent the infectious forms of this parasite and are utilized to evaluate infectivity and cellular entry [46]. Moreover, in contrast to epimastigotes, trypomastigotes exhibit high resistance to numerous drugs. Consequently, based on the findings discussed above, these results are promising and suggest a set of comTo a solution of **7a** demonstrated in subsequent experiments.

To explain the eventual structure–activity relationship (SAR) between the chemical structures of purines, a detailed analysis is presented in the following sections.

3.1.1. SAR for NINOA strain

It should be noted that although most of these compounds were more active than Bzn and Nfx, it was still possible to conduct a comparative analysis of the trypanocidal effects of these trisubstituted purines against one another to assess the influence of substitution patterns.

For the NINOA strain, the presence of trifluoromethoxy substituents at R_2 or R_3 (purines **9e**, **9 m**, and **9 n**) was consistently associated with enhanced activity. Likewise, the incorporation of a benzyl group at R_2 (compound **9 t**) produced the most active derivative in the series. In contrast, multiple halogenations, particularly the presence of two adjacent chlorine substituents (compound **9p**), markedly reduced the activity. Methoxy substitutions showed variable effects depending on their position within the aminophenyl moiety at C-6 of the purine scaffold, as evidenced by the comparison according to evidence between **9f–h** and **9i–j**.

Interestingly, the substitution of a hydrogen atom with a fluorine atom at the *meta*-position of the phenylamino group at C-2 of the purine reduced the activity in several cases, for example, when comparing **9a** and **9b**, **9e** and **9 m**, **9i** and **9j**, and **9 g** and **9 h**. The exception was **9c** and **9d**.

3.1.2. SAR for INC-5 strain

Similar SAR trends were observed for INC-5. Compound **9t** again displayed the highest activity, whereas purines containing trifluoromethoxy or methoxy substituents generally exhibited improved potency (**9i**, **9j**, **9m,** and **9n**). The relative position and nature of the halogen substituents strongly influenced the activity, indicating that both steric and electronic effects contributed to the trypanocidal profile of these derivatives. Like what was observed for NINOA, the substitution of a hydrogen atom with a fluorine atom at the *meta*-position of the phenylamino fragment at C-2 of the purine decreased trypanocidal activity. Fig. 3 summarises the results obtained in this study, considering both SAR analyses.

3.2. Trypanocidal activity of selected purine derivatives against Tulahuen-2 T. cruzi amastigotes and cytotoxicity on Vero cells

To further evaluate the biological relevance of the most active compounds, selected purine derivatives were tested against intracellular amastigotes of the Tulahuen-2 strain and subjected to cytotoxicity assays in Vero cells. The selected purines were **9e**, **9i**, **9j**, **9 m**, **9 n**, and **9 t**, as they had the lowest IC_{50} values for trypomastigotes in every strain. As amastigotes require host cells to develop, it was necessary to consider the toxicity of the compounds on Vero cells; therefore, a viability assay was also performed.

As shown in Table 2, all tested derivatives exhibited trypanocidal activity at concentrations below 10 μM, except for compound **9i**. Notably, **9 m** was the most active of these purines (IC_{50} = 1.82 μM), compared to Bzn (IC_{50} = 2.92 μM). From a chemical point of view, this suggests that trypanocidal activity on amastigotes is favoured only when there is monosubstitution in the *para*-position relative to the phenylamino group at C-6 of the purine, as observed for **9e**, **9m**, **9n**, and **9t**. Considering these findings, it is crucial to highlight that **9 m** demonstrates significant potential because of its trypanocidal activity against intracellular amastigotes. These amastigotes represent the primary form of intracellular replication responsible for tissue damage in human Chagas disease. Pharmacological research aimed at developing novel therapeutics against *T. cruzi* prioritizes this phase due to its substantial clinical significance, necessitating the selection of drugs capable of permeating the host cell membrane [47]. Additionally, certain amastigotes may enter a latent or "persistent" state, akin to that of tuberculosis, rendering them less susceptible to Bzn or Nfx. Consequently, a comprehensive and contemporary drug discovery strategy for *T. cruzi* should employ amastigote models, particularly mammalian cell lines, as a primary screening method. This approach is essential because studies involving epimastigotes frequently yield false positives owing to their heightened susceptibility and distinct metabolic processes [48,49].

In contrast, as expected, given their multiple mechanisms of action reported, all purine derivatives showed measurable cytotoxicity in Vero cells. However, purines **9 m** and **9 t** had the highest CC_{50} values, resulting in higher selectivity index (SI) values (6.5 and 3.7, respectively). Although the IC_{50} values of these purines in Vero cells were no higher than those of the reference drugs, this is a factor that must be considered when designing future purine derivatives, with the aim of increasing this SI to ensure low cytotoxicity in mammalian cells. Nevertheless, the one-digit micromolar anti-*T. cruzi* activities observed for this series of purine derivatives are in good agreement with those reported in previous studies for this family of compounds, although the selectivity indices are narrow [19].

Currently, two commonly accepted criteria for the progression of compounds in HTS phenotypic cascades against *T. cruzi* are $IC_{50} < 5$ μM and SI > 10 [48]. Five of the purine derivatives evaluated here meet the first criterion, demonstrating the potential of the purine scaffold for antiparasitic applications. However, most compounds also elicited moderate cytotoxicity in Vero cells, which could be attributed to their previously described activity on various important targets and processes in cancer cell lines [26,27,50]. In this regard, a certain level of toxicity is expected in non-target-specific chemical series, such as the one used in this study. It is worth noting that repositioned hits in their initial stages, showing 3 < SI < 5, can eventually advance to hit-to-lead optimization [51,52], on the premise that subsequent medicinal chemistry efforts will improve their selectivity/cytotoxicity profiles. In this context, purine derivatives **9 m** and **9 t** clearly excel over the rest of the candidates as interesting starting points for future optimization, considering both: (i) their micromolar activity against the infective (*i.e.*, trypomastigotes) and replicative (*i.e.*, amastigotes) forms of *T. cruzi* parasites from different strains and DTU (*Tc*I for NINOA and INC-5, and *Tc*VI for Tul

Table 3
In vitro activity of selected purine derivatives against *Tc*CZP and *Tc*BDF2.

Compound	IC_{50} *Tc*CZP (μM)	K_d *Tc*BDF2 (μM)
9e	404	ND
9i	205.3	13.5 ± 1.2
9j	87.1	ND
9m	257	ND
9n	197.3	ND
9t	234.1	19.6 ± 1.2

ND, not determined; the compound was inactive at the highest evaluated concentration.

strain), and (ii) their suitable selectivity indices over Vero cells.

3.3. Identification of targets: in vitro activity against TcCZP and TcBDF2

To determine the possible mechanism of action of the compounds and to probe our initial hypothesis based on bibliographic antecedents [20–25], we evaluated the activity of the compounds against *Tc*CZP and *Tc*BDF2. The selected compounds were purines that exhibited the highest activity against *T. cruzi* trypomastigotes (Table 1). These compounds were tested *in vitro* to determine their experimental activities, and the results are summarised in Table 3.

First, all six derivatives (**9e**, **9i**, **9j**, **9m**, **9n**, and **9t**) showed only slight potential to act as *Tc*CZP inhibitors. Despite these purines displaying typical dose-response curves (Fig. S1), the activity observed for these purine derivatives as inhibitors was very low, with IC_{50} values of 87.1–404 μM, with the most active being **9j** (87.1 μM). However, the concentrations required for enzyme inhibition were substantially higher than those associated with trypanocidal activity, suggesting that *Tc*CZP inhibition is unlikely to fully explain the observed effects on the cells.

In contrast, bromodomains do not have enzymatic activity but rather a capacity to bind to acetylated lysines. To determine the activity of the compounds against *Tc*BDF2, their ability to bind bromodomains was evaluated using a melting-point assay. Because the assay requires significant amounts of recombinant protein, an initial screening was performed using a fixed concentration (5 μM). Only compounds **9i** and **9t**, which showed a change in melting temperature greater than 0.5 °C at this concentration, were used to calculate the affinity constants. Thus, the K_d values obtained for compounds **9i** and **9j** were 13.5 and 19.6 μM, respectively (Table 3, Fig. S2). Furthermore, the K_d values obtained for **9i** and **9t** are like those obtained for other bromodomain inhibitors with trypanocidal activity such as bromosporin (BSP) or iBET151 and therefore may justify the trypanocidal activity of these compounds [53, 54]. In addition, *Tc*BDF3, an atypical member of the BET bromodomain family in *T. cruzi*, previously characterised [53], was evaluated using a thermal shift assay at a fixed concentration of 5 μM for the selected compounds (Fig. S2). Under these conditions, no significant thermal shift was observed, suggesting a lack of detectable interaction with *Tc*BDF3, in contrast to the binding observed for *Tc*BDF2. These results suggest a degree of selectivity toward *Tc*BDF2 over *Tc*BDF3 for the evaluated compounds in this study.

The inhibition of *Tc*BDF2 may be related to its observed trypanocidal activity, as the concentrations required for target inhibition and parasite death are in a similar range. Importantly, our data rule out the inhibition of *Tc*CZP and *Tc*BDF-2 as the antiparasitic mode of action of purine derivative **9m**, which is the most promising hit from phenotypic screening. As most of these compounds were originally designed to target the ATP-binding site of human tyrosine kinases Bcr-Abl and Btk [27], and *T. cruzi* genome completely lacks tyrosine kinases [55,56], many targets bearing a similar ATP-binding site might function as off-targets for this compound. This was recently reported for dasatinib, an inhibitor of human Src/Abl tyrosine protein kinase, which binds to the kinase domain of the unrelated TcK2 protein kinase of *T. cruzi* and inhibits parasite replication at sub-micromolar concentrations [57]. Putative targets for this compound might also include *T. cruzi* hypoxanthine-guanine phosphoribosyl transferase enzyme, recently postulated as the putative target of purine-based anti-*T. cruzi* compounds [19].

3.4. Molecular docking studies

To explain why these purine derivatives exhibited low *Tc*CZP inhibition and improved binding to *Tc*BDF2, initial docking studies were conducted. To assess the potential binding mode and determine how it compares to known inhibitors for both proposed targets, molecular docking was performed for the most active *Tc*CZP and *Tc*BDF2 inhibitors **9j**, and **9i** respectively.

3.4.1. Analysis for the interaction with T. cruzi cruzain (TcCZ)

Purine derivative **9j** was docked at the site of a known *Tc*CZ inhibitor (*N*-(1*H*-benzimidazol-2-yl)-1,3-dimethyl-pyrazole-4-carboxamide), referred to as **3H5**, as described in the PDB database. A blind-binding protocol was used to explore alternative binding sites. As shown in Fig. S3, both directed and blind-binding protocols were used for the **9j** derivative. The best position for each protocol was found in the pocket occupied by the known *Tc*CZ inhibitor **3H5**, suggesting that **9j** binds similarly to **3H5**, blocking access to the *Tc*CZ catalytic site. Therefore, once it was proposed that the potential binding site in *Tc*CZ for **9j** was the same as that of the co-crystallised ligand, **9j** was compared with inhibitor **VII** (Fig. 2), which served as the reference purine for this study. Fig. 4**A–D** show the interaction profiles of inhibitor **VII** and purine **9j**, providing information on the possible binding mode of **9j**, which shares the same interactions as **VII**, such as with SER25 and GLN19.

However, although they possess similar interactions and binding energy values, this does not explain the low activity of **9j** compared to that of **VII**. Therefore, the hypotheses to consider are as follows: i) The influence of the fragment attached to C-2 of the purine, where for **VII**, it is small—only the nitrile group—but for **9j**, it is a phenylamino group attached in position to an *N*-methylpiperazine, which is oriented through the solvent-exposed region. This clear difference in volume must be the main reason for the lower enzymatic activity. However, it is important to remember that although **VII** is a good inhibitor of *Tc*CZP, it has low activity against *T. cruzi*. ii) The inhibitory potency of **9j** can be explained, at least partially, by the significant molecular differences between *Tc*CZ (a single, recombinant, non-glycosylated variant lacking the C-terminal domain), used as a docking template, and endogenous cruzipain (a mixture of multiple glycosylated variants occurring within the parasite) [58], which was used in this study for inhibition experiments.

3.4.2. Analysis for the interaction with TcBDF2

Purine derivative **9i** was docked at the site of the known bromodomain inhibitor **BSP**, as reported in the Protein Data Bank database, in addition to using a blind protocol. As shown in Fig. 5**A**, both site-directed and blind protocols were followed for docking purine **9i**. The best pose for each protocol was in the cavity occupied by the known *Tc*BDF2 inhibitor **BSP**, suggesting that **9i** may act similarly to **BSP** by hindering access to the bromodomain residues. The binding energy observed for **9i** was slightly better than that of **BSP** for both protocols, which coincided with a slightly lower K_d for this compound than that previously reported for BSP for *Tc*BDF3 [54]. Fig. 5**B–D** show the interaction profiles for the known inhibitor **BSP** and the newly discovered inhibitor **9 i**, providing insight into the potential binding mode of **9i**, which shares three to four interacting residues with the target protein. Moreover, Fig. 5**E** shows the crystal poses for **BSP**, and the top pose for each docking protocol has the purine ring nearly overlapping, further emphasising the benefit of the scaffold for developing potential inhibitors. The overlap of the three molecules shows that the purine ring is directed toward the active-site cavity. In the case of purine derivatives, the cyclopropylmethyl group reaches in, permitting an additional interaction with PHE31, which may help stabilise the complex with

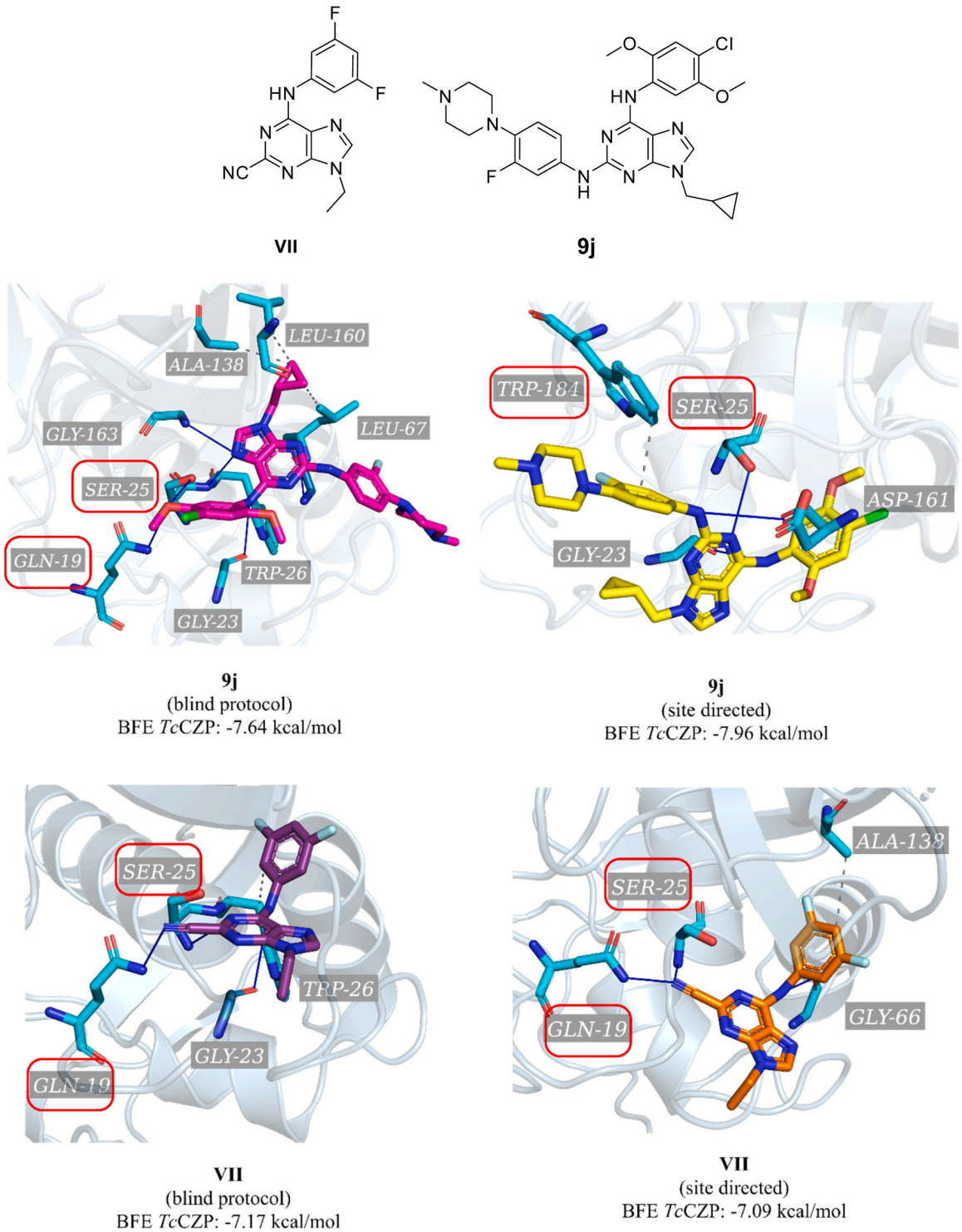

Fig. 4. Summary of the docking analysis of purine derivatives **9j** and **VII**. Independent interaction profiles, hydrogen bonds (blue), and hydrophobic bonds (grey dotted). The red boxes highlight the shared interacting residues.

*Tc*BDF2. These results indicate that *Tc*BDF2 could be a target of action that justifies the trypanocidal activity of compound **9i** (and perhaps of other purine derivatives used in this study).

3.5. Molecular dynamics analysis on TcBDF2

Molecular dynamics (MD) studies were conducted to investigate the fact that **9i** is a better *Tc*BDF2 ligand. To achieve this goal, the potentially stable binding modes of both ligands in complexes with these proteins were evaluated. A 200 ns molecular dynamics simulation was performed for the most energetically favourable docking pose of this ligand. Three analyses were performed on the obtained trajectory: root-mean-square fluctuation (RMSD), root-mean-square fluctuation (RMSF), and radius of gyration (RoG). The resultant graphical representations are presented below.

The root-mean-square fluctuation (RMDS) was calculated for the apo-protein structure, holo-protein (in complex with the inhibitor), and purine **9i** trajectory throughout the 200 ns trajectory, and a graphical

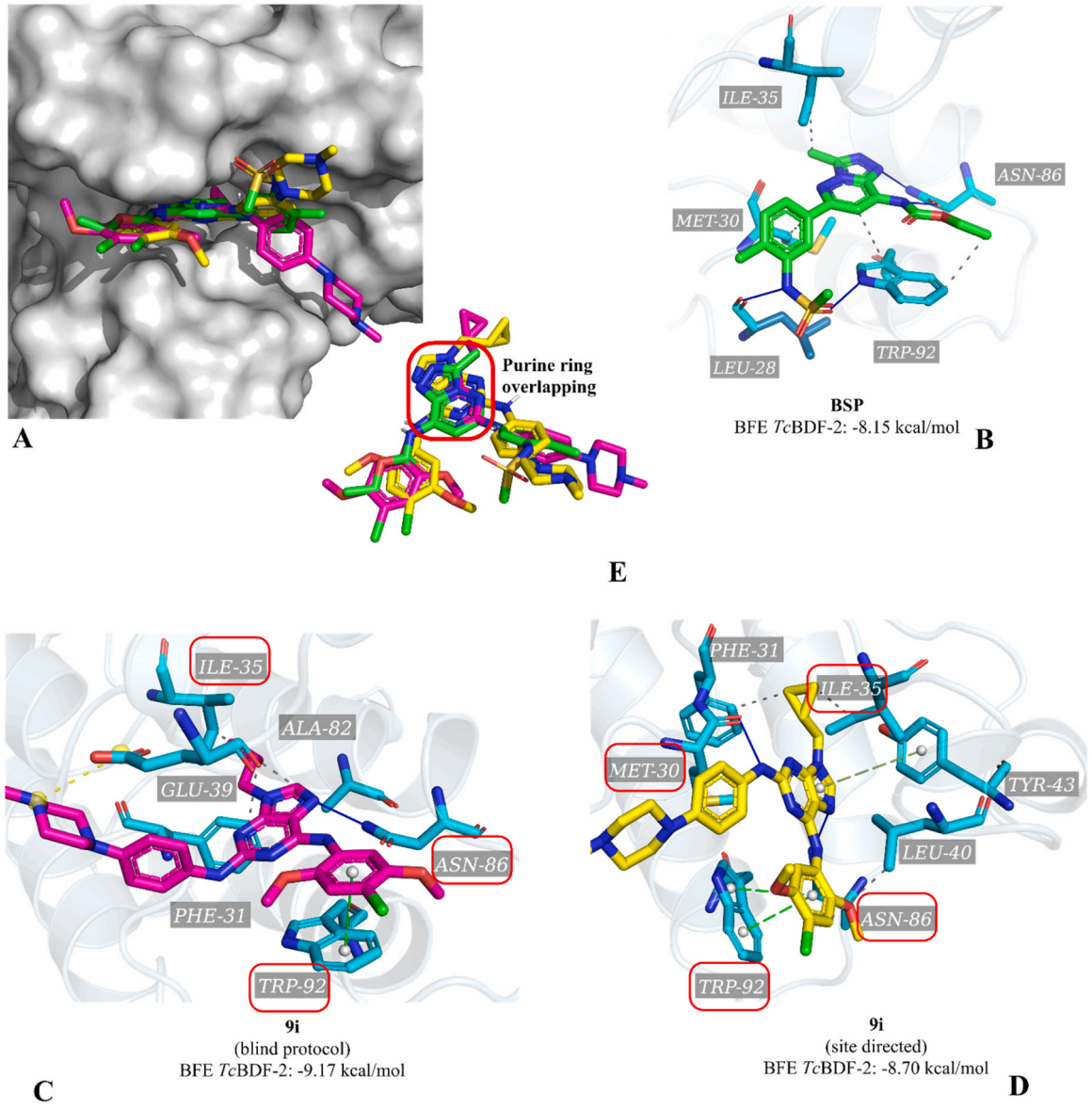

Fig. 5. Summary of the docking analysis of **BSP** and purine **9i**. **A)** Overlapping of derivative **9i** blind (magenta), site-directed (yellow), and BSP [crystal pose] (green) protocols, and **BSP** [crystal pose] (green). **B–D)** Independent interaction profiles, hydrogen bonds (blue), hydrophobic bonds (grey dotted), salt bridges (yellow), and π-cation interactions (green). **E)** Figure depicting the overlap of purine rings of BMF and the top poses for blind and site-directed docking protocols. The red boxes highlight the shared interacting residues.

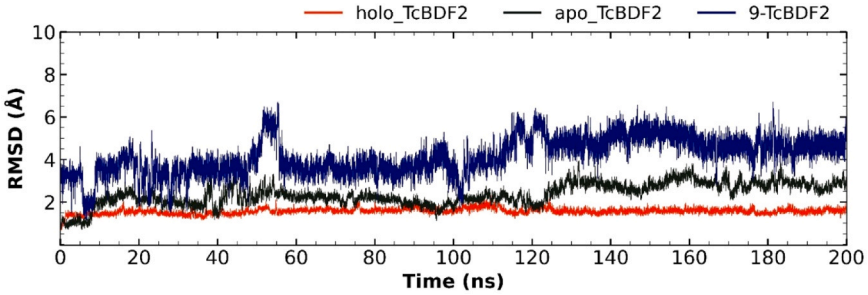

Fig. 6. RMSD graphical representation of the apo-(black), holo-(red), and **9i** (blue) proteins for the apo-protein (black), holo-protein (red), and **9i** (blue) molecular dynamics' trajectories of *Tc*BDF2.

representation is shown (Fig. 6). It may be observed that the holo-protein ($\bar{x}$ = 1.57 ± 0.14 Å) has a slightly more stable behaviour than the apo-protein ($\bar{x}$ = 2.36 ± 0.51 Å), thus it may be suggested that the binding of **9i** allows for an increased structural stability. The trajectory for **9i** ($\bar{x}$ = 4.16 ± 0.87 Å) showed fluctuations but maintained a plateau-like behaviour from 125 ns until the end of the dynamics'

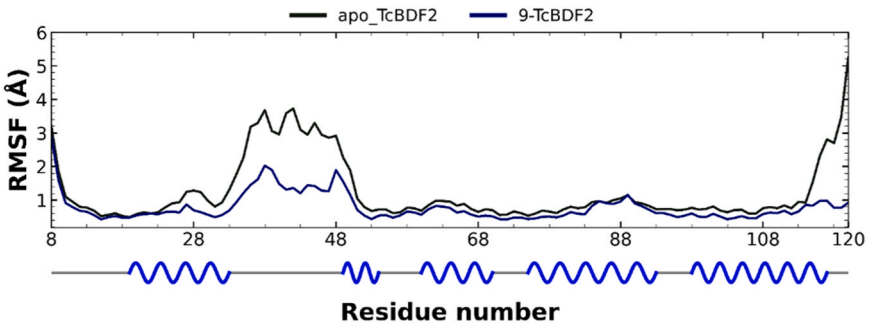

Fig. 7. RMSF graphical representation of the apo- (blue) and holo-protein (**9i**) (black) dynamics' trajectory. The secondary structural elements of *Tc*BDF2 are annotated with blue sinusoidal lines (α-helices) and grey lines (unstructured regions).

Table 4
Predicted molecular properties, ADME parameters, and toxicity of compounds **9i**, **9j**, **9 m,** and **9 t**.

Compound	MW (Da)	HBA	HBD	cLogP	TPSA (Å^2)	NRB	hERG	CYP Substrate	Pgp Inhibition
Desirable value	≤ 500	≤ 10	≤ 5	≤ 5	≤ 140	≤ 10	M or L	-	Yes
9i	549.07	6	2	4.08	92.60	9	M	2D6	Yes
9j	567.06	7	2	4.36	92.60	9	M	2C9/2C19	Yes
9m	538.57	8	2	4.33	87.37	9	M	2C9/2C19/3A4	Yes
9t	544.69	4	2	4.96	74.14	9	M	2C9/2C19/3A4	Yes

The predicted values were obtained from the SwissADME website (http://www.swissadme.ch/index.php). hERG, *in vitro* human ether-a-go-go-related gene channel inhibition. M and L indicate medium- and low-risk, respectively. hERG inhibition, CYP, and Pgp estimations were calculated using PreADMET (https://preadmet.webservice.bmdrc.org/toxicity/).

trajectory. Overall, this analysis suggests that **9i** behaves as an inhibitor and maintains a binding pose close to the initial docking position.

As a pertinent analysis for the dynamics' trajectory analysis, the root-mean-square fluctuation (RMSF) was determined, and the overall fluctuations are presented in Fig. 7.

The RMSF graph, as presented in Fig. 7, shows a prominent fluctuation in the residue range 33–48 which belongs to a loop (unstructured) region, consistent with the tendency of unstructured regions to be more prone to fluctuations. Notably, the graphs show increased stability for the holo-protein in this region, which is part of the binding site of the protein. This behaviour suggests that the binding of **9i** is stable, as it permits an increase in stability. This is consistent with *in vitro* findings showing an affinity for **9i**. The radii of gyration for the apo- and holo-proteins (bound to **9i**) are presented in Fig. S4, which shows that there is no major change in the radius of gyration between both forms of the protein: apo ($\bar{x}$=13.92 ± 0.25 Å) and holo ($\bar{x}$=13.74 ± 0.08 Å); thus, binding to **9i** does not alter the compactness of the protein.

3.6. Predicted physicochemical and ADME properties

One key aspect to consider in the search for antiparasitic drugs is their pharmacokinetic (PK) properties. In addition to cytotoxic properties, mechanism of action, and cell death, the physicochemical properties that influence drug absorption, distribution, metabolism, and excretion (ADME) must also be considered. Thus, these properties can be considered during the optimisation of bioactive compounds, ultimately making them suitable candidates for preclinical studies [59]. To assess the physicochemical properties of purines **9i**, **9j**, **9m**, and **9t**, the free online platform SwissADME (http://www.swissadme.ch/index.php) was used in accordance with Lipinski and Veber rules [60,61]. According to these criteria, the four purines exhibited promising permeability and bioavailability owing to their HBD, HBA, and cLogP values. However, their MW values were close to the optimum limit [60]. Additionally, these four purines had a topological polar surface area (TPSA) and a number of rotatable bonds (NRB) values that were both less than 140 Å^2 and ≤ 10 NRB, respectively (Table 4), which met the criteria set forth by Veber's rules [61]. Based on the results provided by both models, it can be concluded that these purines have a high potential to penetrate cell membranes and demonstrate good oral absorption. Furthermore, the bioavailability radar plot generated by the SwissADME platform suggested that the purines exhibit good oral absorption (Fig. 8). Regarding toxicity, these four purines were predicted to moderately inhibit hERG potassium ion channels. This can be explained by the pharmacophores present in these purines, which are typical of known hERG inhibitors; these usually include basic, positively charged nitrogen atoms rather than acidic or neutral functional groups. However, certain chemical strategies can be used to redesign compounds with a reduced effect on hERG, such as decreasing their lipophilicity and basicity and increasing their rigidity, which will be considered for new purines [62]. Finally, these purines are expected to be substrates for some CYP, as indicated in Table 4, suggesting metabolic stability against first-pass metabolism. For P-glycoprotein (Pgp), which acts as an efflux pump, it is desirable for these purines to inhibit this transporter to enhance intestinal absorption and achieve higher intracellular concentrations in host cells, as well as ADME and toxicity.

4. Conclusions

In this study, 20 purine derivatives were evaluated *in vitro* against trypomastigote forms of two Mexican strains of *T. cruzi*. The trypanocidal activity of these compounds against both forms, and in most cases, was better than that of Bzn and Nfx, especially compound **9t**, which showed the lowest IC_{50} values for both the strains. The six most promising purine derivatives were tested against the amastigote form of *T. cruzi*, and four were active at concentrations below 10 μM, with purine **9m** having the lowest IC_{50} and the best, even low, SI. The purine derivatives that had the greatest effect on trypomastigotes were not effective *Tc*CZP inhibitors, as initially speculated. Conversely, purines **9i** and **9t** showed *Tc*BDF2 K_d values of 13.5 and 19.6 μM, respectively, consistent with their trypanocidal activity, as well as with the affinity constant of previously reported trypanocidal bromodomain inhibitors. Furthermore, compounds **9i** and **9t** did not exhibit binding affinity to *Tc*BDF3, demonstrating selectivity among these targets. Likewise, docking and molecular dynamics studies showed that **9i** stably binds to

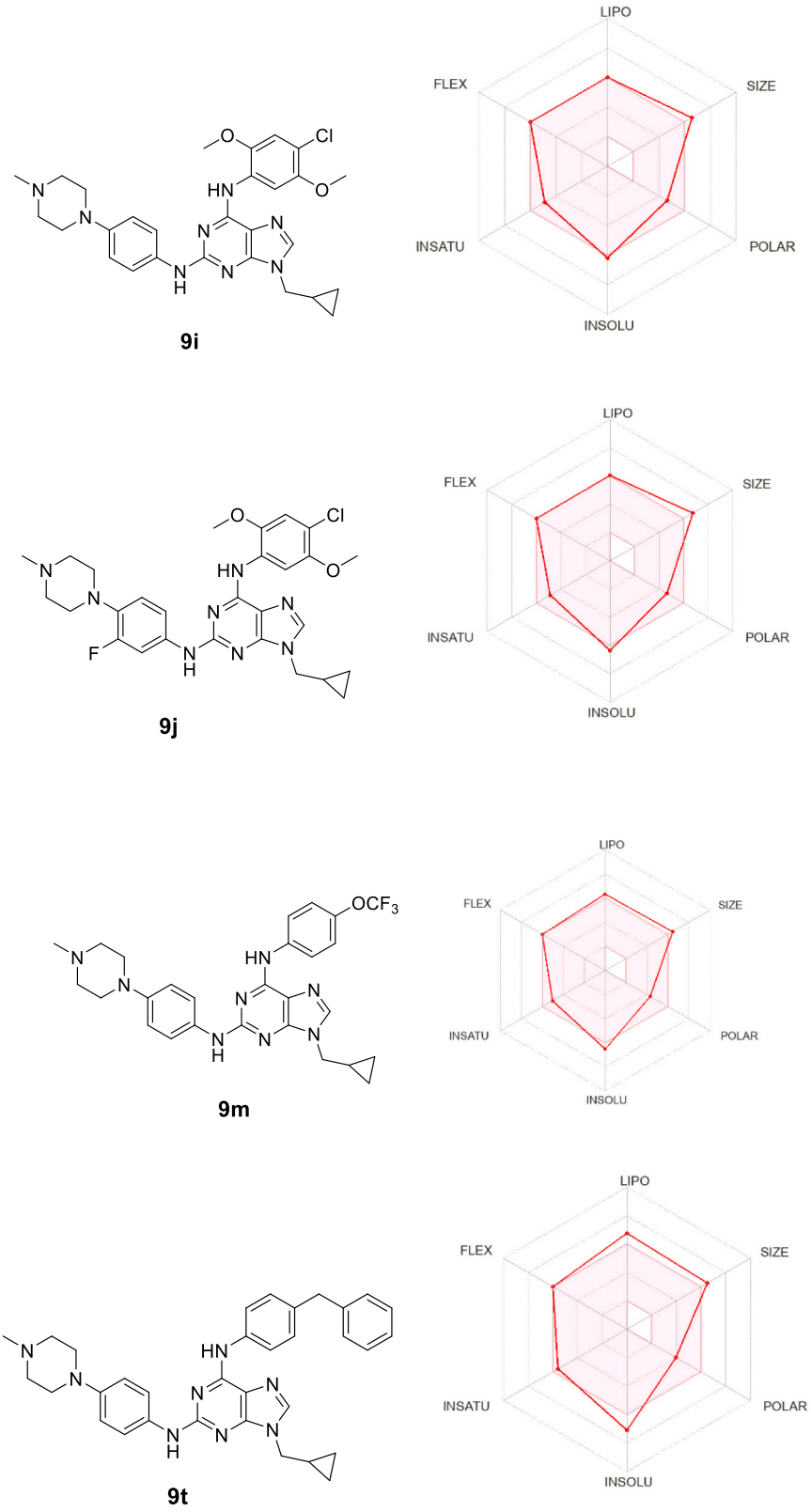

Fig. 8. Radar chart illustrating the bioavailability of **9i**, **9j**, **9m**, and **9t**. The pink range represents the optimal values for each property related to oral bioavailability. The forecasted properties, marked in red, include flexibility (FLEX), lipophilicity (LIPO), solubility (INSOLU), size (SIZE), polarity (POLAR), and saturation (INSATU). If all parameters fall within the designated range, the compound is anticipated to exhibit good oral absorption.

the hydrophobic pocket of *Tc*BDF2. This interaction occurs through the purine ring, at the same position as the purine-like ring of BSP, validating the usefulness of the purine scaffold as a strategy for developing bromodomain inhibitors as trypanocidal agents.

Therefore, we acknowledge that the main limitation of this study was the low SI obtained when evaluating the biological activity of the compounds analysed. To address this issue, our group is currently developing future strategies. These include the use of excipients or nanoformulations, the modification of the most active compounds into prodrugs, and conjugation, among other approaches. Furthermore, as new potential targets responsible for trypanocidal activity are identified—such as for **9t**—we will gain a more comprehensive understanding of certain key structural patterns of these compounds. This understanding will enable the redesign of more potent and safer compounds based on the purine scaffold. However, it should be recognized that future efforts will be made possible by this initial breakthrough presented in this work.

CRediT authorship contribution statement

Garnham Mercedes: Visualization, Investigation. **Emir Salas-Sarduy:** Writing – review & editing, Visualization, Supervision, Funding acquisition, Formal analysis. **Gildardo Rivera:** Writing – review & editing, Writing – original draft, Visualization, Supervision, Resources, Project administration, Funding acquisition. **Victoria Alonso:** Writing – review & editing, Visualization, Investigation, Formal analysis. **Esteban Serra:** Writing – review & editing, Supervision, Funding acquisition. **Gǿmez-Escobedo Rogelio:** Visualization, Investigation, Formal analysis. **Jean-Luc Bertrand:** Investigation. **Benjamín Nogueda-Torres:** Writing – review & editing, Supervision, Funding acquisition. **Cristian O. Salas:** Writing – review & editing, Writing – original draft, Visualization, Supervision, Resources, Project administration, Funding acquisition, Conceptualization. **Delgado Thalia:** Writing – review & editing, Visualization, Investigation. **Alonzo González-González:** Writing – original draft, Visualization, Investigation.

Ethical certifications

The animal study protocol was approved by the Institutional Review Board of the Instituto Politécnico Nacional (protocol code ZOO-006-2020 and date of approval 20 December 2020).

Declaration of Competing Interest

The authors declare the following financial interests/personal relationships which may be considered as potential competing interests: Cristian O. Salas reports that financial support was provided by FONDECYT (N° 1231199).

Acknowledgements

The authors thank Dr. Frederick Buckner for donating transgenic Tulahuen β-galactosidase parasites used in this study.

Appendix A. Supporting information

Supplementary data associated with this article can be found in the online version at doi:10.1016/j.biopha.2026.119636.

Data availability

Data will be made available on request.

References

[1] C. Bern, Chagas' disease, N. Engl. J. Med. 373 (2015) 456–466, https://doi.org/10.1056/NEJMra1410150.
[2] L. Briceno, W. Mosca, [What is not searched, it is difficult to find: Chagas' disease, G Ital. Cardiol. 17 (2016) 343–347, https://doi.org/10.1714/2252.24258.
[3] M.A. Rajao, C. Furtado, C.L. Alves, D.G. Passos-Silva, M.B. de Moura, B. L. Schamber-Reis, M. Kunrath-Lima, A.A. Zuma, J.P. Vieira-da-Rocha, J.B. Garcia, et al., Unveiling benznidazole's mechanism of action through overexpression of DNA repair proteins in Trypanosoma cruzi, Environ. Mol. Mutagen. 55 (2014) 309–321, https://doi.org/10.1002/em.21839.
[4] F. He, J. Shi, Y. Wang, S. Wang, J. Chen, X. Gan, B. Song, D. Hu, Synthesis, antiviral activity, and mechanisms of purine nucleoside derivatives containing a sulfonamide moiety, J. Agric. Food Chem. 67 (2019) 8459–8467, https://doi.org/10.1021/acs.jafc.9b02681.
[5] L.P. Jordheim, D. Durantel, F. Zoulim, C. Dumontet, Advances in the development of nucleoside and nucleotide analogues for cancer and viral diseases, Nat. Rev. Drug. Discov. 12 (2013) 447–464, https://doi.org/10.1038/nrd4010.
[6] C.M. Galmarini, J.R. Mackey, C. Dumontet, Nucleoside analogues and nucleobases in cancer treatment, Lancet Oncol. 3 (2002) 415–424, https://doi.org/10.1016/s1470-2045(02)00788-x.
[7] C. Wei, L. Zhou, Y. Yang, L. Niu, H. Yan, Design, synthesis, and anticancer evaluation of N(6) -hydrazone purine derivatives with potential antiplatelet aggregation activity, Chem. Biol. Drug. Des. 101 (2023) 568–580, https://doi.org/10.1111/cbdd.14145.
[8] Y. Hu, S. Hu, G. Pan, D. Wu, T. Wang, C. Yu, M. Fawad Ansari, R.R. Yadav Bheemanaboina, Y. Cheng, L. Bai, et al., Potential antibacterial ethanol-bridged purine azole hybrids as dual-targeting inhibitors of MRSA, Bioorg. Chem. 114 (2021) 105096, https://doi.org/10.1016/j.bioorg.2021.105096.
[9] S.S. Krajewski, I. Isoz, J. Johansson, Antibacterial and antivirulence effect of 6-N-hydroxylaminopurine in Listeria monocytogenes, Nucleic Acids Res. 45 (2017) 1914–1924, https://doi.org/10.1093/nar/gkw1308.
[10] S. Konduri, J. Prashanth, V.S. Krishna, D. Sriram, J.N. Behera, D. Siegel, K.P. Rao, Design and synthesis of purine connected piperazine derivatives as novel inhibitors of Mycobacterium tuberculosis, Bioorg. Med. Chem. Lett. 30 (2020) 127512, https://doi.org/10.1016/j.bmcl.2020.127512.
[11] F. Hulpia, G.D. Campagnaro, K.J. Alzahrani, I.A. Alfayez, M.A. Ungogo, D. Mabille, L. Maes, H.P. de Koning, G. Caljon, S. Van Calenbergh, Structure-activity relationship exploration ᵐ°of 3′-deoxy-7-deazapurine nucleoside analogues as anti-Trypanosoma brucei agents, ACS Infect. Dis. 6 (2020) 2045–2056, https://doi.org/10.1021/acsinfecdis.0c00105.
[12] V.H. Nguyen, M. Tichy, S. Rozankova, R. Pohl, A.M. Downey, E. Dolezelova, E. Tloustova, M. Slapnickova, A. Zikova, M. Hocek, Synthesis and anti-trypanosomal activity of 3′-fluororibonucleosides derived from 7-deazapurine nucleosides, Bioorg. Med. Chem. Lett. 40 (2021) 127957, https://doi.org/10.1016/j.bmcl.2021.127957.
[13] S. Azzouz, P. Lawton, In vitro effects of purine and pyrimidine analogues on Leishmania donovani and Leishmania infantum promastigotes and intracellular amastigotes, Acta Parasitol. 62 (2017) 582–588, https://doi.org/10.1515/ap-2017-0070.
[14] J. Bouton, A. Furquim d′Almeida, L. Maes, G. Caljon, S. Van Calenbergh, F. Hulpia, Synthesis and evaluation of 3′-fluorinated 7-deazapurine nucleosides as antikinetoplastid agents, Eur. J. Med. Chem. 216 (2021) 113290, https://doi.org/10.1016/j.ejmech.2021.113290.
[15] F. Hulpia, K. Van Hecke, C. Franca da Silva, D. da Gama Jaen Batista, L. Maes, G. Caljon, C.S.M. de Nazare, S. Van Calenbergh, Discovery of novel 7-aryl 7-deazapurine 3′-deoxy-ribofuranosyl nucleosides with potent activity against Trypanosoma cruzi, J. Med. Chem. 61 (2018) 9287–9300, https://doi.org/10.1021/acs.jmedchem.8b00999.
[16] C. Lin, F. Hulpia, C.F. da Silva, D. Batista, K. Van Hecke, L. Maes, G. Caljon, M.N. C. Soeiro, S. Van Calenbergh, Discovery of pyrrolo[2,3-b]pyridine (1,7-dideazapurine) nucleoside analogues as anti-Trypanosoma cruzi agents, J. Med. Chem. 62 (2019) 8847–8865, https://doi.org/10.1021/acs.jmedchem.9b01275.
[17] C. Lin, D.D.G. Jaen Batista, A.L. Mazzeti, R. Donola Girao, G.M. de Oliveira, I. Karalic, F. Hulpia, M.N.C. Soeiro, L. Maes, G. Caljon, et al., N(6)-modification of 7-deazapurine nucleoside analogues as Anti-Trypanosoma cruzi and anti-Leishmania agents: structure-activity relationship exploration and In vivo evaluation, Eur. J. Med. Chem. 231 (2022) 114165, https://doi.org/10.1016/j.ejmech.2022.114165.
[18] B. Barnadas-Carceller, N. Martinez-Peinado, L.C. Gomez, A. Ros-Lucas, J. C. Gabaldon-Figueira, J.J. Diaz-Mochon, J. Gascon, I.J. Molina, Y.V.M.J. Pineda de Las Infantas, J. Alonso-Padilla, Identification of compounds with activity against Trypanosoma cruzi within a collection of synthetic nucleoside analogs, Front. Cell. Infect. Microbiol. 12 (2022) 1067461, https://doi.org/10.3389/fcimb.2022.1067461.
[19] N. Martinez-Peinado, A. Lorente-Macias, A. Garcia-Salguero, N. Cortes-Serra, A. Fenollar-Collado, A. Ros-Lucas, J. Gascon, M.J. Pinazo, I.J. Molina, A. Unciti-Broceta, et al., Novel purine chemotypes with activity against Plasmodium falciparum and Trypanosoma cruzi, Pharmaceuticals 14 (2021), https://doi.org/10.3390/ph14070638.
[20] M.H. Branquinha, S.S. Oliveira, L.S. Sangenito, C.L. Sodre, L.F. Kneipp, C. M. d'Avila-Levy, A.L. Santos, Cruzipain: an update on its potential as chemotherapy target against the human pathogen Trypanosoma cruzi, Curr. Med. Chem. 22 (2015) 2225–2235, https://doi.org/10.2174/0929867322666150521091652.
[21] L. Lima, P.A. Ortiz, F.M. da Silva, J.M. Alves, M.G. Serrano, A.P. Cortez, S. C. Alfieri, G.A. Buck, M.M. Teixeira, Repertoire, genealogy and genomic

organization of cruzipain and homologous genes in Trypanosoma cruzi, T. cruzi-like and other trypanosome species, PLoS One 7 (2012) e38385, https://doi.org/10.1371/journal.pone.0038385.
[22] B.T. Mott, R.S. Ferreira, A. Simeonov, A. Jadhav, K.K. Ang, W. Leister, M. Shen, J. T. Silveira, P.S. Doyle, M.R. Arkin, et al., Identification and optimization of inhibitors of Trypanosomal cysteine proteases: cruzain, rhodesain, and TbCatB, J. Med. Chem. 53 (2010) 52–60, https://doi.org/10.1021/jm901069a.
[23] L.E. Tavernelli, V.L. Alonso, I. Pena, E. Rodriguez Araya, R. Manarin, J. Cantizani, J. Martin, J. Salamanca, P. Bamborough, F. Calderon, et al., Identification of novel bromodomain inhibitors of Trypanosoma cruzi bromodomain factor 2 (TcBDF2) using a fluorescence polarization-based high-throughput assay, Antimicrob. Agents Chemother. 68 (2024) e0024324, https://doi.org/10.1128/aac.00243-24.
[24] V.L. Alonso, A.M. Escalante, E. Rodriguez Araya, G. Frattini, L.E. Tavernelli, D. M. Moreno, R.L.E. Furlan, E. Serra, 1,3,4-oxadiazoles as inhibitors of the atypical member of the BET family bromodomain factor 3 from Trypanosoma cruzi (TcBDF3), Front. Microbiol. 15 (2024) 1465672, https://doi.org/10.3389/fmicb.2024.1465672.
[25] G.V. Villanova, S.C. Nardelli, P. Cribb, A. Magdaleno, A.M. Silber, M.C. Motta, S. Schenkman, E. Serra, Trypanosoma cruzi bromodomain factor 2 (BDF2) binds to acetylated histones and is accumulated after UV irradiation, Int. J. Parasitol. 39 (2009) 665–673, https://doi.org/10.1016/j.ijpara.2008.11.013.
[26] J. Bertrand, H. Dostalova, V. Krystof, R. Jorda, T. Delgado, A. Castro-Alvarez, J. Mella, D. Cabezas, M. Faundez, C. Espinosa-Bustos, et al., Design, synthesis, in silico studies and inhibitory activity towards Bcr-Abl, BTK and FLT3-ITD of new 2,6,9-trisubstituted purine derivatives as potential agents for the treatment of leukaemia, Pharmaceutics 14 (2022), https://doi.org/10.3390/pharmaceutics14061294.
[27] J. Bertrand, H. Dostalova, V. Krystof, R. Jorda, A. Castro, J. Mella, C. Espinosa-Bustos, A. Maria Zarate, C.O. Salas, New 2,6,9-trisubstituted purine derivatives as Bcr-Abl and Btk inhibitors and as promising agents against leukemia, Bioorg. Chem. 94 (2020) 103361, https://doi.org/10.1016/j.bioorg.2019.103361.
[28] K. Domingues, A. de Fátima, M. Fachi, R.E. Luna Lazo, L. Ferreira, R. Pontarolo, Drug repurposing for trypanosomiasis: using machine learning models and polypharmacology to identify multitarget candidates, J. Braz. Chem. Soc. 36 (2025), https://doi.org/10.21577/0103-5053.20250028.
[29] M. Sulik, D. Otto-Ślusarczyk, D. Steverding, M. Struga, A. Huczyński, Antiproliferative and trypanocidal activity of ivermectin bioconjugates, ACS Omega 10 (2025) 27380–27392, https://doi.org/10.1021/acsomega.5c02998.
[30] Z. Blanco, E. Fernandez-Moreira, M.R. Mijares, C. Celis, G. Martínez, J.B. De Sanctis, S. Gurská, P. Džubák, M. Hajdůch, A. Mijoba, et al., Synthesis, leishmanicidal, trypanocidal, antiproliferative assay and apoptotic induction of (2-phenoxypyridin-3-yl)naphthalene-1(2h)-one derivatives, Molecules 27 (2022) 5626.
[31] Nd.J. Hiller, N.A.Ae Silva, R.X. Faria, A.L.A. Souza, J.A.L.C. Resende, A. Borges Farias, N. Correia Romeiro, D. de Luna Martins, Synthesis and evaluation of the anticancer and trypanocidal activities of boronic tyrphostins, ChemMedChem 13 (2018) 1395–1404, https://doi.org/10.1002/cmdc.201800206.
[32] J.P. Jourdan, R. Bureau, C. Rochais, P. Dallemagne, Drug repositioning: a brief overview, J. Pharm. Pharmacol. 72 (2020) 1145–1151, https://doi.org/10.1111/jphp.13273.
[33] Z. Brener, Therapeutic activity and criterion of cure on mice experimentally infected with Trypanosoma cruzi, Rev. Inst. Med. Trop. Sao Paulo 4 (1962) 389–396.
[34] F.S. Buckner, C.L. Verlinde, A.C. La Flamme, W.C. Van Voorhis, Efficient technique for screening drugs for activity against Trypanosoma cruzi using parasites expressing beta-galactosidase, Antimicrob. Agents Chemother. 40 (1996) 2592–2597, https://doi.org/10.1128/AAC.40.11.2592.
[35] S.A. Ahmed, R.M. Gogal Jr., J.E. Walsh, A new rapid and simple non-radioactive assay to monitor and determine the proliferation of lymphocytes: an alternative to [3H]thymidine incorporation assay, J. Immunol. Methods 170 (1994) 211–224, https://doi.org/10.1016/0022-1759(94)90396-4.
[36] F. Parussini, M. Garcia, J. Mucci, F. Aguero, D. Sanchez, U. Hellman, L. Aslund, J. J. Cazzulo, Characterization of a lysosomal serine carboxypeptidase from Trypanosoma cruzi, Mol. Biochem. Parasitol. 131 (2003) 11–23, https://doi.org/10.1016/s0166-6851(03)00175-0.
[37] E. Salas-Sarduy, L.U. Landaburu, J. Karpiak, K.P. Madauss, J.J. Cazzulo, F. Aguero, V.E. Alvarez, Novel scaffolds for inhibition of Cruzipain identified from high-throughput screening of anti-kinetoplastid chemical boxes, Sci. Rep. 7 (2017) 12073, https://doi.org/10.1038/s41598-017-12170-4.
[38] V.L. Alonso, C. Ritagliati, P. Cribb, J.A. Cricco, E.C. Serra, Overexpression of bromodomain factor 3 in Trypanosoma cruzi (TcBDF3) affects differentiation of the parasite and protects it against bromodomain inhibitors, FEBS J. 283 (2016) 2051–2066, https://doi.org/10.1111/febs.13719.
[39] N.M. O'Boyle, M. Banck, C.A. James, C. Morley, T. Vandermeersch, G.R. Hutchison, Open Babel: an open chemical toolbox, J. Cheminf. 3 (2011) 33, https://doi.org/10.1186/1758-2946-3-33.
[40] E.F. Pettersen, T.D. Goddard, C.C. Huang, G.S. Couch, D.M. Greenblatt, E.C. Meng, T.E. Ferrin, UCSF chimera–a visualization system for exploratory research and analysis, J. Comput. Chem. 25 (2004) 1605–1612, https://doi.org/10.1002/jcc.20084.
[41] A.T. McNutt, P. Francoeur, R. Aggarwal, T. Masuda, R. Meli, M. Ragoza, J. Sunseri, D.R. Koes, GNINA 1.0: molecular docking with deep learning, J. Cheminf. 13 (2021) 43, https://doi.org/10.1186/s13321-021-00522-2.
[42] M.F. Adasme, K.L. Linnemann, S.N. Bolz, F. Kaiser, S. Salentin, V.J. Haupt, M. Schroeder, PLIP 2021: expanding the scope of the protein-ligand interaction profiler to DNA and RNA, Nucleic Acids Res. 49 (2021) W530–W534, https://doi.org/10.1093/nar/gkab294.
[43] M.J. Abraham, T. Murtola, R. Schulz, S. Páll, J.C. Smith, B. Hess, E. Lindahl, GROMACS: high performance molecular simulations through multi-level parallelism from laptops to supercomputers, SoftwareX 1-2 (2015) 19–25, https://doi.org/10.1016/j.softx.2015.06.001.
[44] P. Polishchuk, A. Kutlushina, D. Bashirova, O. Mokshyna, T. Madzhidov, Virtual screening using pharmacophore models retrieved from molecular dynamic simulations, Int. J. Mol. Sci. 20 (2019), https://doi.org/10.3390/ijms20235834.
[45] A. Majeau, L. Murphy, C. Herrera, E. Dumonteil, Assessing Trypanosoma cruzi parasite diversity through comparative genomics: implications for disease epidemiology and diagnostics, Pathogens 10 (2021), https://doi.org/10.3390/pathogens10020212.
[46] Alonso, V.L., Manarin, R., Perdomo, V., Gulin, E., Serra, E., Cribb, P., In Vitro Drug Screening Against all Life Cycle Stages of Trypanosoma cruzi Using Parasites Expressing β-galactosidase, 1940-087X, vol. 177, 2021, p. e63210.
[47] M.L. Sykes, E.K. Kennedy, V.M. Avery, Impact of laboratory-adapted intracellular Trypanosoma cruzi strains on the activity profiles of compounds with anti-T. cruzi activity, Microorganisms 11 (2023) 476.
[48] J.C. Gabaldon-Figueira, N. Martinez-Peinado, E. Escabia, A. Ros-Lucas, E. Chatelain, I. Scandale, J. Gascon, M.J. Pinazo, J. Alonso-Padilla, State-of-the-art in the drug discovery pathway for Chagas disease: a framework for drug development and target validation, Res. Rep. Trop. Med. 14 (2023) 1–19, https://doi.org/10.2147/RRTM.S415273.
[49] Y. Takagi, Y. Akutsu, M. Doi, K. Furukawa, Utilization of proliferable extracellular amastigotes for transient gene expression, drug sensitivity assay, and CRISPR/Cas9-mediated gene knockout in Trypanosoma cruzi, PLoS Negl. Trop. Dis. 13 (2019) e0007088, https://doi.org/10.1371/journal.pntd.0007088.
[50] A. Chaurasiya, S.K. Wahan, C. Sahu, P.A. Chawla, An insight into the rational design of recent purine-based scaffolds in targeting various cancer pathways, J. Mol. Struct. 1274 (2023) 134308, https://doi.org/10.1016/j.molstruc.2022.134308.
[51] D.A. Otta, F.F. de Araujo, V.B. de Rezende, E.M. Souza-Fagundes, S.M. Eloi-Santos, M.F. Costa-Silva, R.A. Santos, H.A. Costa, J.L. Siqueira-Neto, O.A. Martins-Filho, et al., Identification of anti-Trypanosoma cruzi lead compounds with putative immunomodulatory activity, Antimicrob. Agents Chemother. 62 (2018), https://doi.org/10.1128/AAC.01834-17.
[52] M. Didier Garnham, F.A. Aguero, J.C. Ramirez, F. Aguero, E. Salas-Sarduy, Identification of antifungal agents AR-12 and fosmanogepix as anti-Trypanosoma cruzi drugs through an enhanced fluorogenic beta-galactosidase phenotypic screening assay, ACS Infect. Dis. 12 (2026) 724–737, https://doi.org/10.1021/acsinfecdis.5c00900.
[53] V.L. Alonso, A.M. Escalante, E. Rodríguez Araya, G. Frattini, L.E. Tavernelli, D. M. Moreno, R.L.E. Furlan, E. Serra, 1,3,4-oxadiazoles as inhibitors of the atypical member of the BET family bromodomain factor 3 from Trypanosoma cruzi (TcBDF3), Front. Microbiol. 15 (2024) 2024, https://doi.org/10.3389/fmicb.2024.1465672.
[54] A. Pezza, L.E. Tavernelli, V.L. Alonso, V. Perdomo, R. Gabarro, R. Prinjha, E. Rodriguez Araya, I. Rioja, R. Docampo, F. Calderon, et al., Essential bromodomain TcBDF2 as a drug target against Chagas disease, ACS Infect. Dis. 8 (2022) 1062–1074, https://doi.org/10.1021/acsinfecdis.2c00057.
[55] C. Naula, M. Parsons, J.C. Mottram, Protein kinases as drug targets in trypanosomes and Leishmania, Biochim. Biophys. Acta 1754 (2005) 151–159, https://doi.org/10.1016/j.bbapap.2005.08.018.
[56] M. Cayla, Y.R. Nievas, K.R. Matthews, J.C. Mottram, Distinguishing functions of trypanosomatid protein kinases, Trends Parasitol. 38 (2022) 950–961, https://doi.org/10.1016/j.pt.2022.08.009.
[57] T.P. Marcelino, A.M. Fala, M.M. da Silva, N. Souza-Melo, A.M. Malvezzi, A. H. Klippel, M. Zoltner, N. Padilla-Mejia, S. Kosto, M.C. Field, et al., Identification of inhibitors for the transmembrane Trypanosoma cruzi eIF2alpha kinase relevant for parasite proliferation, J. Biol. Chem. 299 (2023) 104857, https://doi.org/10.1016/j.jbc.2023.104857.
[58] V.C. Santos, A.E.R. Oliveira, A.C.B. Campos, J.L. Reis-Cunha, D.C. Bartholomeu, S. M.R. Teixeira, A.P.C.A. Lima, R.S. Ferreira, The gene repertoire of the main cysteine protease of Trypanosoma cruzi, cruzipain, reveals four sub-types with distinct active sites, Sci. Rep. 11 (2021) 18231, https://doi.org/10.1038/s41598-021-97490-2.
[59] N.A. Meanwell, Improving drug candidates by design: a focus on physicochemical properties as a means of improving compound disposition and safety, Chem. Res. Toxicol. 24 (2011) 1420–1456, https://doi.org/10.1021/tx200211v.
[60] C.A. Lipinski, F. Lombardo, B.W. Dominy, P.J. Feeney, Experimental and computational approaches to estimate solubility and permeability in drug discovery and development settings1PII of original article: S0169-409X(96)00423-1. The article was originally published in Advanced Drug Delivery Reviews 23 (1997) 3–25.1, Adv. Drug. Deliv. Rev. 46 (2001) 3–26, https://doi.org/10.1016/S0169-409X(00)00129-0.
[61] D.F. Veber, S.R. Johnson, H.-Y. Cheng, B.R. Smith, K.W. Ward, K.D. Kopple, Molecular properties that influence the oral bioavailability of drug candidates, J. Med. Chem. 45 (2002) 2615–2623, https://doi.org/10.1021/jm020017n.
[62] A. Garrido, A. Lepailleur, S.M. Mignani, P. Dallemagne, C. Rochais, hERG toxicity assessment: useful guidelines for drug design, Eur. J. Med. Chem. 195 (2020) 112290, https://doi.org/10.1016/j.ejmech.2020.112290.